JOURNAL OF Materials CHEMISTRY

Synthesis, electrical behaviour, and crystal and electronic band structures of two different phases of the $(SMeEt_2)[Pd(dmit)_2]_2$ salt. Consequences of cationic disorder on the electrical properties†

C. Faulmann,*[a] M.-L. Doublet,*[b] F. Granier,[b] B. Garreau de Bonneval,[a] I. Malfant,[a] J.-P. Legros,[a] T. Togonidze[c] and P. Cassoux[a]

[a]*Laboratoire de Chimie de Coordination, CNRS, 205 route de Narbonne, 31077 Toulouse Cedex, France. E-mail: faulmann@lcc-toulouse.fr*
[b]*Laboratoire de Structure et Dynamique des Systèmes Moléculaires et Solides USTL II, Place Eugène Bataillon, 34095 Montpellier Cedex 5, France. E-mail: doublet@lsd.univ-montp2.fr*
[c]*Institute of Solid State Physics, Russian Academy of Sciences, Chernogolovka, Moscow Distr. 142432, Russia*

Received 7th March 2001, Accepted 27th April 2001
First published as an Advance Article on the web 7th June 2001

The previously mentioned $(SMeEt_2)[Pd(dmit)_2]_2$ (**1**) and the new $(SMeEt_2)_{0.5}[Pd(dmit)_2]$ (**2**) phases are obtained by electrocrystallisation of $(SMeEt_2)_2[Pd(dmit)_2]$ in acetonitrile. The crystal structures of **1** and **2** are determined by X-ray diffraction methods, both at room and low temperatures. Though not previously detected, a cation disorder is evidenced in both phases at room temperature which is removed in **1** at low temperatures. Conductivity measurements show a rather smooth metal to insulator transition in the 150–200 K range for **1** whereas **2** behaves as a semiconductor in the whole range of temperature. Under pressure, the transition of **1** is shifted down to lower temperatures and becomes more abrupt. Electronic band structure calculations (by means of the extended Hückel tight-binding model) show that the cation disorder evidenced in **1** is responsible for two different electron transfers occurring from the $(SMeEt_2)^+$ cation layers to the two crystallographically independent anion layers, resulting thus in the observed room temperature metal-like behaviour of **1**. The ambient pressure phase transition of **1** is shown to be the consequence of a more homogeneous electron transfer, possibly leading to a Mott–Hubbard localised state at low temperatures, as is also the case for **2**. Under pressure, the more abrupt phase transition observed in **1** is believed to originate from a different metallic regime.

Introduction

Among all the transition metal complexes that have been used for preparing molecular conductors, some of those derived from the dmit ligand ($dmit^{2-}$ = 2-thioxo-1,3-dithiole-4,5-dithiolato) are the only ones that have been shown to exhibit superconducting behaviour.[1,2] In these systems, although the conducting $M(dmit)_2$-anion layers offer less variety in their molecular packing than that observed for the radical-cation layers in the organic TTF-based conductors, they are known to exhibit various electronic structures depending on the transition metal used (M = Ni, Pd, Pt). Owing to metal···metal interaction, these $M(dmit)_2$-anion layers are generally described by weakly (M = Ni) or strongly (M = Pd, Pt) dimerised chains.[3] The transport properties of the strongly dimerised $[Pd(dmit)_2]_2$-based systems have been shown to be governed by the antisymmetric combination of the two $Pd(dmit)_2$ HOMOs rather than by the symmetric combination of the two $Pd(dmit)_2$ LUMOs, and thus to take place within the inter-chain direction.[3,4] Moreover, among all reported $Pd(dmit)_2$-based molecular compounds, a wide variety of physical properties have been observed. This indicates that the conducting behaviour of these materials can follow, upon a weak perturbation, either a delocalised or a localised regime. For instance, $(\beta\text{-}NMe_4)[Pd(dmit)_2]_2$[5] and $(PMe_4)[Pd(dmit)_2]_2$[6] exhibit a semiconducting behaviour at room temperature and ambient pressure and the former becomes a metal (and even a superconductor) under pressure. α-TTF$[Pd(dmit)_2]_2$[7–9] and $(NMe_4)[Pt(dmit)_2]_2$[10] undergo a metal to insulator transition at low temperatures. Although the subtle structural and electronic factors governing the physical properties of these salts are still elusive, it is now more and more widely admitted that the counter-ions may play an indirect role on the electronic properties of the anions by affecting the dimer packing, and therefore the topology of the inter-dimer interactions within the conducting slabs.

We had reported in a previous work the synthesis, the characterisation and the electronic structure of the $(SMeEt_2)[Pd(dmit)_2]_2$ phase (**1**), which exhibits a non-continuous electrical behaviour[11] upon cooling. Metallic at room temperature, this phase undergoes a rather smooth metal to insulator transition in the range 150–200 K. Though topologically similar, the electronic structures of the two crystallographically independent and strongly dimerised $Pd(dmit)_2$ layers had been shown to be shifted in energy from one to another and therefore associated with different fillings of their respective Ψ^-_{HOMO}-like bands (*i.e.* the band responsible for the conducting behaviour of the salt). In this work, no reference has been made to the role that the counter-ions could play on the two different donor–acceptor electron transfers, and the metal to insulator transition has been proposed to be associated with electronic localisation. To obtain more insight along this line, it seemed interesting to synthesise better quality crystals of this $(SMeEt_2)[Pd(dmit)_2]_2$ phase (**1**) and investigate

†Electronic supplementary information (ESI) available: Tables of crystallographic data for compounds **1** and **2**. See http://www.rsc.org/suppdata/jm/b1/b102133h/

DOI: 10.1039/b102133h

the low-temperature crystal structure. In the course of these new syntheses, we have evidenced a cationic disorder that had not been previously detected. Moreover, we have simultaneously isolated a new phase, designated here phase **2**, with the same $(SMeEt_2)[Pd(dmit)_2]_2$ stoichiometry (actually, $(SMeEt_2)_{0.5}[Pd(dmit)_2]$), but whose conducting properties and crystal structure are strikingly different. Indeed **2** behaves as a semiconductor over the whole range of temperatures. It thus appeared of particular interest to figure out whether the cationic disorder observed in **1** could be responsible for its metal to insulator transition and if so, whether this feature could be related to the existence of **2**.

We report here on the synthesis, room and low temperature X-ray characterisations, conductivity measurements and electronic band structure calculations of **2** together with resistivity measurements under pressure, and low-temperature X-ray determination of the previously reported phase **1**.[11]

Experimental

Sample preparation

The $(SMeEt_2)_2[Pd(dmit)_2]$ starting complex was synthesised from $dmit(COPh)_2$[12] with $SMeEt_2I$ and Na_2PdCl_4 as a source of counter-ion and metal. Galvanostic electrochemical oxidation (1–3 μA cm^{-2}; platinum electrodes, 1 cm long, 1 mm diameter) of a solution of $(SMeEt_2)_2[Pd(dmit)_2]$ in acetonitrile yielded within a couple of days platelet-like crystals suitable for X-ray analysis and conductivity measurements. As was shown later by X-ray diffraction studies, all samples collected from the anode contain two phases, $(SMeEt_2)[Pd(dmit)_2]_2$ (**1**) and $(SMeEt_2)_{0.5}[Pd(dmit)_2]$ (**2**), which are not morphologically distinguishable since both phases crystallise as platelets and even often as superposed platelets.

X-Ray structure determination

Data collection and cell refinement were performed at room temperature on a CAD4 Enraf–Nonius diffractometer by using the CAD4-Express package[13] and on a IPDS Stoe diffractometer, by using the IPDS software[14] at 160 K. All calculations were carried out using the WinGX package,[15] with SIR92[16] for the solutions and SHELXL97[17] for the subsequent refinements, with all reflections included in the calculations. Drawings were obtained with Cameron.[18] All non-H atoms were refined anisotropically. Positions of H atoms were calculated, with an isotropic displacement parameter 20 or 50% higher than that of the parent atom (methylene or methyl group, respectively).

Crystal structure determination of 1 at 160 K. *Crystal data.* $C_{17}H_{13}Pd_2S_{21}$, $M=1103.58$, triclinic, $a=7.7888(9)$, $b=36.181(3)$, $c=6.2573(6)$ Å, $\alpha=92.112(11)$, $\beta=112.169(12)$, $\gamma=88.740(12)^\circ$, $U=1631.8(3)$ $Å^3$, $T=160$ K, space group $P\bar{1}$ (no. 2), $Z=2$, $\mu(MoK\alpha)=2.463$, 9065 reflections measured, 3336 unique ($R_{int}=0.059$) which were all used in all calculations. The final R and $wR(F^2)$ are 0.096 and 0.229, respectively (all data).

Crystal structure determination of 1 at room temperature. *Crystal data.* Since this structure has already been reported[11] but without the disorder on the cation, hereafter are only given the R values when considering this latter structural feature: the final R and $wR(F^2)$ are 0.102 and 0.199, respectively (based on F^2 (all data)), or 0.065 and 0.171 for data such as $I>2\sigma(I)$ (based on F^2) to be compared with 0.074 and 0.079 (based on F). CCDC reference number 162839–162842. See http://www.rsc.org/suppdata/jm/b1/b102133h/ for crystallographic files in .cif format.

Crystal structure determination of 2 at 160 K. *Crystal data.* $C_{17}H_{13}Pd_2S_{21}$, $M=1103.58$, triclinic, $a=7.7877(12)$, $b=18.323(3)$, $c=6.2846(10)$ Å, $\alpha=96.80(2)$, $\beta=112.257(18)$, $\gamma=84.17(2)^\circ$, $U=822.5(2)$ $Å^3$, $T=160$ K, space group $P\bar{1}$ (no. 2), $Z=1$, $\mu(MoK\alpha)=2.463$, 6587 reflections measured, 2415 unique ($R_{int}=0.042$) which were all used in all calculations. The final R and $wR(F^2)$ are 0.037 and 0.093, respectively (all data).

Crystal structure determination of 2 at room temperature. *Crystal data.* Triclinic, $a=7.844(5)$, $b=18.397(5)$, $c=6.320(5)$ Å, $\alpha=97.654(5)$, $\beta=112.076(5)$, $\gamma=83.572(5)^\circ$, $U=835.7(9)$ $Å^3$, space group $P\bar{1}$ (no. 2), $Z=1$, 4847 unique reflections measured ($R_{int}=0.00$), which were all used in all calculations. The final R and $wR(F^2)$ are 0.057 and 0.079, respectively (all data). CCDC reference number 162839–162842. See http://www.rsc.org/suppdata/jm/b1/b102133h/ for crystallographic files in .cif format.

Conductivity measurements at ambient pressure and under pressure

Ambient-pressure, temperature-dependent (300–304 K) single crystal conductivity measurements were performed with the standard four-probe-method using the same devices previously described.[11] For measurements under pressure, quasi-hydrostatic pressure was applied using a BeCu clamp cell with mineral oil GKZh-94 as a pressure medium. The pressure was estimated from the applied loading force at room temperature and corrected for low temperatures according to Thompson.[19]

Band structure calculations

The electronic band structures of the anion layers of **1** and **2** were investigated using full tight-binding calculations based upon the effective one-electron Hamiltonian of the extended Hückel model.[20] The off-diagonal matrix elements of the Hamiltonian β_{ij} were calculated according to the modified Wolfsberg–Helmotz formula.[21] All valence electrons were explicitly treated in the calculations and the basis set, consisting of single-ζ Slater-type orbitals for all atoms, was taken from previous work.[22]

Results and discussion

X-Ray descriptions

Phase 1 at room temperature. Except the disorder of the sulfonium cation, which had not been detected in the previous description,[11] no additional important changes are to be pointed out in the re-determination of this crystal structure. The asymmetric unit of phase **1** contains two crystallographically independent $Pd(dmit)_2$ units (1 and 2) and one $(SMeEt_2)^+$ cation (Fig. 1), whose methyl groups are disordered on two positions. Due to the relative arrangement of the two independent $Pd(dmit)_2$ units, this content leads to a herringbone stacking arrangement in the *ab* plane as shown in Fig. 2. Each independent $Pd(dmit)_2$ unit forms segregated stacks in the [100] direction. Within each stack, the $Pd(dmit)_2$ units are paired through a Pd···Pd bond (3.130(3) and 3.139(3) Å for 1 and 2, respectively). The adjacent stacks are connected through short S···S contacts (Table 1), hence forming layers of $[Pd(dmit)_2]_2$ diads in the *ac* plane. The $Pd(dmit)_2$ units are eclipsed within a pair with an inter-planar distance almost identical for Pd(1) and Pd(2) (3.501 and 3.505 Å, respectively), whereas they are slipped between pairs, with an inter-planar distance slightly larger between Pd(1) pairs (3.587 Å) than between Pd(2) pairs (3.578 Å).

Although connected to each other through one S···S contact involving one terminal S atom along the [010] direction (S15···S30: 3.513(7) Å), the layers built on each independent $Pd(dmit)_2$ unit are separated from each other by sheets of disordered cations. The disorder concerns only the methyl groups of the sulfonium cation: these groups are equally

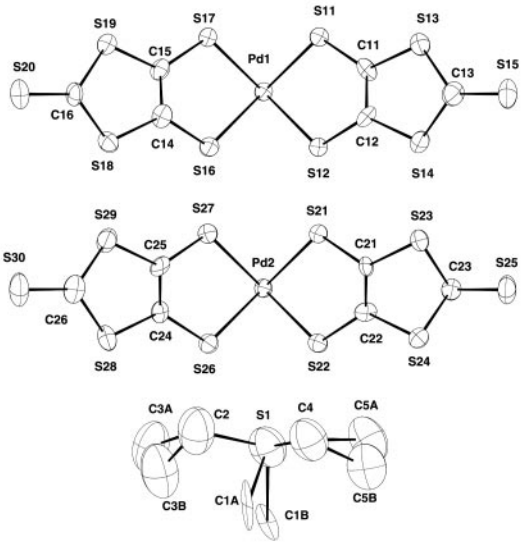

Fig. 1 Atomic numbering scheme for $(SMeEt_2)[Pd(dmit)_2]_2$ (**1**).

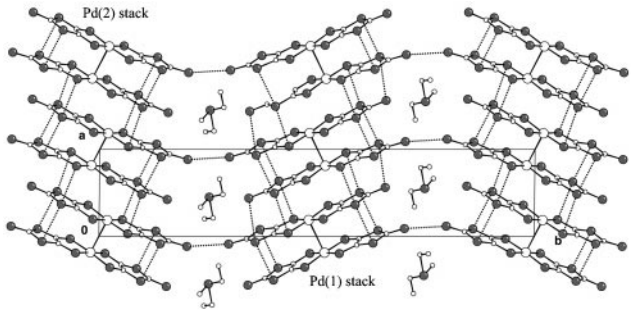

Fig. 2 Projection of the structure of **1** onto the *ab*-plane.

Table 1 Intermolecular short S···S distances (<3.70 Å) between the $Pd(dmit)_2$ units in $(SMeEt_2)[Pd(dmit)_2]_2$ (**1**) at room temperature and at 160 K

	Distance/Å	
Atoms	Room temp.	160 K
S11···S12	3.5305(67)	3.4963(102)
S11···S14	3.5776(62)	3.5433(94)
S11···S16	3.2820(64)	3.2848(94)
S11···S17	3.4734(53)	3.4492(79)
S11···S18	3.6729(67)	3.6544(96)
S11···S19	3.5054(53)	3.4827(74)
S12···S17	3.4366(57)	3.4008(88)
S12···S17	3.2696(65)	3.2819(92)
S12···S19	3.6874(69)	3.6653(99)
S13···S18	3.6274(69)	3.6209(97)
S13···S20	3.6839(72)	3.6915(95)
S14···S19	3.6447(70)	3.6464(99)
S16···S17	3.5142(68)	3.4882(102)
S16···S19	3.4664(60)	3.4333(93)
S17···S17	3.4348(53)	3.4023(73)
S21···S21	3.3898(51)	3.3650(75)
S21···S22	3.5214(66)	3.4806(102)
S21···S26	3.4439(58)	3.4163(92)
S21···S26	3.2745(63)	3.2780(95)
S21···S27	3.4691(52)	3.4350(78)
S22···S23	3.4579(61)	3.4262(95)
S22···S27	3.2985(64)	3.2935(95)
S23···S26	3.6725(68)	3.6486(100)
S23···S27	3.4788(53)	3.4528(74)
S23···S28	3.6436(70)	3.6300(100)
S24···S27	3.6530(66)	3.6322(97)
S24···S29	3.6333(69)	3.6111(99)
S26···S27	3.5228(67)	3.4797(103)
S27···S28	3.5848(65)	3.5573(98)
S15···S30	3.5128(70)	3.5127(104)

distributed over two positions. It should be noted that, for each position of the S-coordinated methyl group, four conformations are observed for the cation since the terminal methyl groups of the ethylenic substituents are also disordered. For the disordered S–Me group, when considering the Et substituents fixed, there are two different orientations of the cation with respect to the out-of-plane main axis of the $Pd(dmit)_2$. The influence of this feature on the electron transfer will be discussed later in the present paper in terms of electronic structural features and physical properties of **1**.

Phase 1 at 160 K. As in the room temperature crystal structure of phase **1**, at 160 K, the asymmetric unit contains two crystallographically independent $Pd(dmit)_2$ and one $(SMeEt_2)^+$ cation unit (whose labelling is similar to that of **1** at room temperature, with C1 instead of C1A and C1B, C3 instead of C3A and C3B and C5 instead of C5A and C5B). It should be noted here that the cation is not disordered any longer. Since there is only one conformation for the cation, there is only one possible orientation of the S–Me axis with respect to each $Pd(dmit)_2$ unit. At first sight, compared to the room temperature crystal structure, no important changes within the intra- and intermolecular distances can be seen at 160 K: the intra- and intermolecular distances do not seem to drastically change, as reflected by the inter-planar distances (within a dimer: 3.497 Å for Pd(1) and 3.492 Å for Pd(2); between dimers: 3.577 Å for Pd(1) and Pd(2)) and by the S···S distances within each stack (Table 1). Nevertheless, a careful examination of the bond lengths reveals slight and subtle changes when going from room temperature to 160 K, particularly as far as the differences between independent units 1 and 2 are considered. Since the esd's of the two structures are identical, their bond lengths can be compared. At 160 K, both units are almost identical: this is reflected not only by the inter-planar distances which tend to become equal at low temperatures, but also by the variation when going from room temperature to 160 K in the differences of sums of selected bond lengths between units 1 and 2 (Table 2): for example, the largest difference for the sum of the four S–C bond lengths of the internal cycle in unit 1 compared to that in unit 2 is only 0.02 Å at 160 K, whereas this difference is larger than 0.05 Å at room temperature. This difference is even more pronounced when considering the difference for the sum of the two central C=C bond lengths: 0.01 Å at 160 K and 0.07 Å at room temperature. Even when taking into account the values of the esd's of the considered bond lengths, these variations clearly indicate that the two independent units in **1** can be considered as different at room temperature whereas they are almost identical at 160 K.

Phase 2 at 160 K. The asymmetric unit of **2** contains one $Pd(dmit)_2$ unit and one-half $(SMeEt_2)^+$ cation close to the middle of the *a*-edge. The labelling of the $Pd(dmit)_2$ unit and $(SMeEt_2)^+$ cation are similar to that of the Pd(1) unit and sulfonium cation in **1** at 160 K, respectively (see Fig. 1). Due to its position, the occupation of the cation is only 0.5. Like in phase **1**, the $Pd(dmit)_2$ units are paired through a Pd···Pd bond

Table 2 Comparison of bond lengths (Å) in $(SMeEt_2)[Pd(dmit)_2]_2$ (**1**) at room temperature and 160 K

	Room temperature			160 K		
	Layer 1	Layer 2	δ	Layer 1	Layer 2	δ
Σ(Pd)S–C	6.73	6.79	−0.06	6.94	6.92	0.02
ΣC=C	2.76	2.69	0.07	2.64	2.65	−0.01

Σ(Pd)S–C = sum of the four S–C bond lengths of the internal cycles. ΣC=C = sum of the two C=C bond lengths. δ = difference between the sums of the involved bond lengths in the two independent units.

Table 3 Short S···S distances (<3.70 Å) between the $Pd(dmit)_2$ units in $(SMeEt_2)_{0.5}[Pd(dmit)_2]$ (**2**) at 160 K

Atoms	Distance/Å
S11···S11	3.3867(18)
S11···S12	3.5114(22)
S11···S16	3.4301(18)
S11···S16	3.2801(20)
S11···S17	3.4276(18)
S12···S12	3.5102(18)
S12···S13	3.4403(19)
S12···S16	3.5889(18)
S12···S17	3.3045(20)
S13···S16	3.6593(21)
S13···S17	3.4503(17)
S13···S18	3.6426(21)
S14···S16	3.4974(18)
S14···S17	3.6496(21)
S14···S18	3.6682(19)
S14···S19	3.6430(22)
S16···S17	3.4959(21)
S17···S18	3.5844(19)
S20···S20	3.5063(22)

of 3.1397(9) Å and form segregated stacks along the [100] direction. Adjacent stacks are connected through several S···S contacts (Table 3). The structure consists of layers of $Pd(dmit)_2$ dimers parallel to the *ac* plane separated by sheets of cations also lying in the *ac* plane. Like in **1**, a short S···S interatomic distance (S20···S20: 3.506(2) Å) is observed between neighbouring layers of $Pd(dmit)_2$ units. However, in contrast to **1**, the $Pd(dmit)_2$ units are parallel to each other when going from one layer to the next one along the *b*-direction (Fig. 3). The $Pd(dmit)_2$ units are eclipsed within the dimer and slipped between dimers, with an inter-planar distance of 3.518 and 3.568 Å respectively.

Since the cation lies close to an inversion centre, it can be regarded as disordered. Indeed, the two symmetry-related positions of the cation are not simultaneously occupied. However, in contrast to the disorder observed in **1** at room temperature, the present disorder leads to the same orientation of the S–Me axis with respect to the $Pd(dmit)_2$ normal axis.

Phase 2 at room temperature. The structure of **2** at room temperature does not show any significant difference with the structure at 160 K. The inter-planar distances within and between dimers are 3.538 and 3.599 Å, respectively, with a Pd···Pd distance of 3.1534(18) Å within a dimer. The intramolecular and intermolecular distances are given in the electronic supplementary information (ESI).†

Comparison of phases 1 and 2. From a crystallographic point of view, the main difference between the structural arrangement of **1** and **2** lies in the orientation of the $Pd(dmit)_2$ dimers in the adjacent stacks. In **2**, these units are always parallel to each other whereas they form an angle of 131.15° at 293 K and 130.91° at 160 K in **1**. One might wonder whether phase **2** just results from an irreversible structural phase transition undergone by **1** upon cooling. To check this hypothesis, we have determined the cell parameters of several crystals, first at room temperature, then by slowly lowering the temperature and simultaneously checking the cell parameters every 20 K down to 120 K, and then once again at room temperature. The cooling process was carried out over two days, *i.e.*, slowly enough in order not to freeze any unstable intermediate structural state. None of the two phases showed any sign of a transition into the other one.

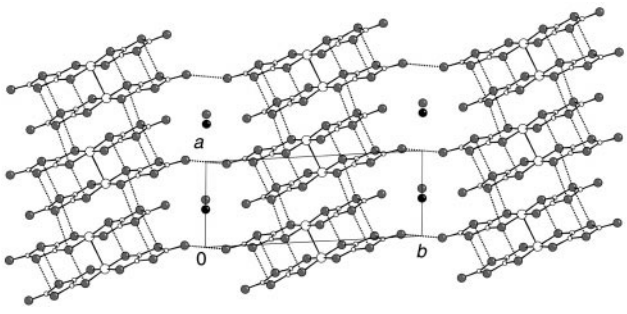

Fig. 3 Projection of the structure of **2** onto the *ab*-plane (only the S atom of the cations are shown for reasons of clarity, and the black and grey S atoms have an occupancy of 50%).

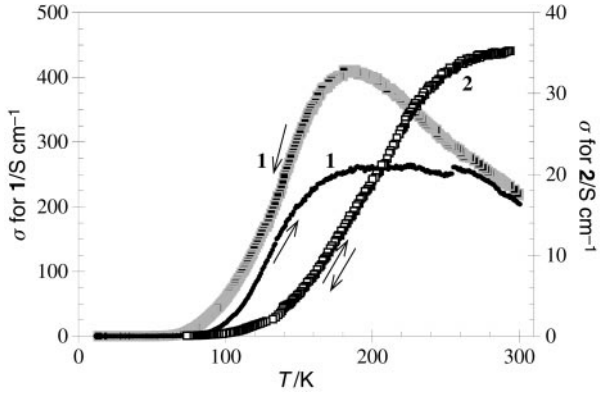

Fig. 4 Temperature dependence of the conductivity of **1** and **2**.

Electrical behaviour

The room temperature conductivity of **1** lies in the range 70–220 S cm^{-1}. Compound **1** exhibits a metal-like behaviour from room temperature down to *ca.* 150–200 K and behaves below these temperatures like a semiconductor (Fig. 4). This behaviour is not reversible since, in the subsequent warming up cycle, the semiconductor behaviour may be maintained up to *ca.* 270 K (or even up to room temperature). Unlike **1**, **2** behaves like a semiconductor from room temperature down to 70 K (Fig. 4). This behaviour is fully reversible. The room temperature conductivity lies in the range 10–40 S cm^{-1} and the activation energy is *ca.* 0.06 eV.

Applying pressure to **1** results in a shift of the metal to insulator transition down to the low temperature region and the transition becomes more abrupt (Fig. 5). It should be noted that applying pressure also results in restoring the reversibility of the electrical behaviour, at 4.8 kbar as well as 9.6 kbar.

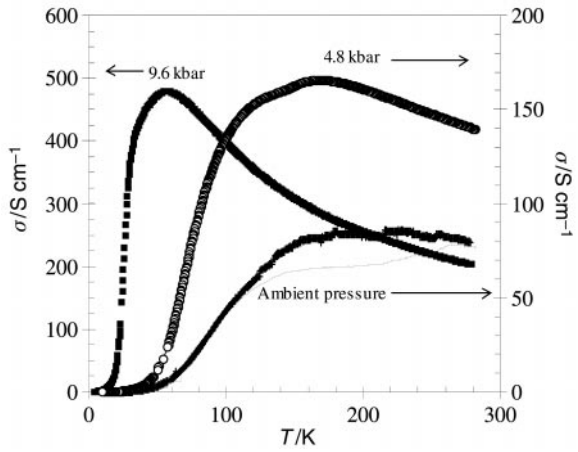

Fig. 5 Temperature dependence under pressure of the conductivity of **1**.

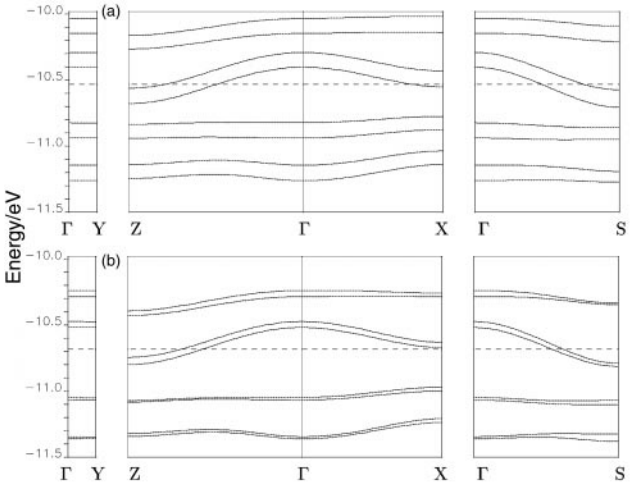

Fig. 6 Three-dimensional electronic band structure of the anionic part of **1** for the room-temperature (a) and the low-temperature (b) crystal structures. Γ, X, Y, Z, S correspond to the (0,0,0), (a*/2,0,0), (0,b*/2,0), (0,0,c*/2), ($-a$*/2,0,c*/2) k-vectors of the first Brillouin zone. The dotted horizontal line stands for the Fermi level associated with the total $[Pd(dmit)_2]_4^{2-}$ electron transfer ($\rho=-1$, *i.e.*, $\rho\approx-1/2$ per layer).

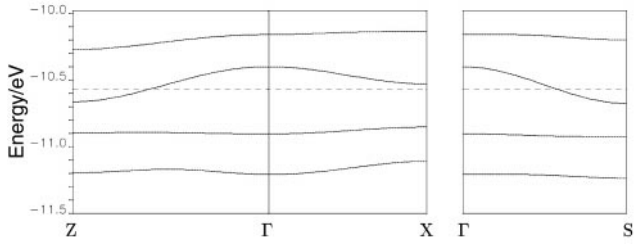

Fig. 7 Two-dimensional electronic band structure of the anionic part of **2** for the room-temperature crystal structure. Γ, X, Z, S correspond to the (0,0), (a*/2,0), (0,c*/2), ($-a$*/2,c*/2) k-vectors of the first Brillouin zone. The dotted horizontal line stands for the Fermi level associated with the total $[Pd(dmit)_2]_2^{1-}$ electron transfer ($\rho=-1/2$).

Electronic band structures

Fig. 6 shows the electronic band structure of the anion part of **1**, both at room temperature (Fig. 6a) and at low temperature (Fig. 6b). A 2D electronic band structure had been previously reported for **1** at room temperature.[11] The aim of the present 3D band calculations was to explicitly account for possible inter-layer $Pd(dmit)_2\cdots Pd(dmit)_2$ interactions. As previously suggested from the 293 K electronic band structure of **1**,[11] the 3D calculations confirm that these interactions are negligible in the whole range of temperatures. The eight bands presented on the two electronic band structures of Fig. 6 consist of four pairs of equivalent bands. Moreover, all bands are flat along the inter-layer b direction, *i.e.* in the ΓY section of the band diagram. An interesting point to be noticed is that the energy shift observed between the two anion layers at room temperature strongly decreases at low temperatures. As a consequence, the two different electron transfers expected to occur at room temperature between the cation slabs and the two independent anion layers ($\rho=-1/3$ for layer 1 and $\rho=-2/3$ for layer 2) become progressively equal when the temperature is lowered. This confirms that the metal to insulator transition observed for **1** around 150–200 K is the result of a more homogeneous electron transfer from the cations to the anionic layers ($\rho\approx-1/2$), as previously suggested by Canadell and coworkers.[11] Moreover, whereas the highest bands of each pair correspond to layer 1 at room temperature, they correspond to layer 2 at low temperatures, suggesting that the main changes induced by the transition concern layer 1.

The Fermi level associated with a total $[Pd(dmit)_2]_4^{2-}$ electron transfer ($\rho=-1$) lies in the almost degenerate and weakly dispersive Ψ^-_{HOMO}-bands of the two anion layers, leading to almost equivalent electron transfers for the two slabs ($\rho\sim-1/2$). This is corroborated by the very similar intramolecular distances reported at low temperatures for the two independent $Pd(dmit)_2$ units of **1**.[23] As previously reported[11] the Fermi surface of the two layers associated with a $\rho=-1/2$ electron transfer exhibit a pseudo one-dimensional character in agreement with either a metallic behaviour (with a better conductivity along the c direction) or a Mott–Hubbard localised state. These two hypotheses are consistent with the fact that the metal to insulator transition temperature is shifted down to lower temperatures when pressure is applied. However, since no structural modulation of the crystal structure of **1** has been evidenced down to very low temperatures, it is likely that the localised semiconducting state is preferred for **1** at low temperatures and ambient pressure.

The electronic structure of the anion layers of **2** confirms this hypothesis. Indeed, as shown in Fig. 7, it resembles the electronic structure of **1** in all directions of the Brillouin zone, indicating that the anion layers are topologically equivalent in **1** and **2**. Moreover, unlike the two anion layers of **1** that are slightly stabilised when temperature decreases (see Fig. 6), the unique anion layer of **2** remains unchanged from 293 to 160 K, in agreement with its stable physical behaviour down to very low temperatures. A superimposition of the room temperature band structures of **1** and **2** shows that the anion layer of **2** lies in energy between the two anion layers of **1**. This confirms that three different electron transfers have to be considered in these two different phases, *i.e.*, $\rho=-1/3$ (layer 1) and $\rho=-2/3$ (layer 2) for **1** and $\rho=-1/2$ for **2**.

For a better understanding of these various electron transfers, closer attention should be drawn to the cations. One may indeed envision in both phases an actual influence of the cation disorder on the electron transfer by focussing on the different $Pd(dmit)_2$ environments with respect to the cations. As mentioned above in the crystallographic section, the cationic disorder observed in **1** (at 293 K) induces two different orientations of the S—Me bond axis. The angle (α) calculated between this S—Me bond and the out-of-plane normal axis of each $Pd(dmit)_2$ unit are reported in Table 4, both at room and at low temperatures. Since each anion layer is surrounded by two cation layers related by an inversion centre, the two angles calculated for one $Pd(dmit)_2$ unit and its two neighbouring cations are complementary to one another. This clearly shows that, at room temperature, the two independent $Pd(dmit)_2$ units of **1** exhibit different environments with respect to the $S—Me^1$ cation, and rather similar ones with respect to the $S—Me^2$ cation. When the temperature decreases, the cation ordering occurring in **1** leads to almost equivalent environments for the two independent $Pd(dmit)_2$ units. The angles calculated at 160 K are similar to that found at room temperature for

Table 4 Angles (°) measured between the different S–Me bond axes and the out-of-plane $Pd(dmit)_2$ principal axis in **1** and **2**, both for the room- and the low-temperature crystal structures. For one layer environment, the two angles that one $Pd(dmit)_2$ molecule makes with its two neighbouring cations have to be considered

	1				**2**	
	$T=293$K		$T=160$K		$T=293$K	$T=160$K
	Layer 1	Layer 2	Layer 1	Layer 2	Pd	Pd
$S—Me^1$	87.46	67.14	—	—	—	—
$S—Me^1_i$	92.54	112.86	—	—	—	—
$S—Me^2$	63.34	107.47	63.47	107.48	75.74	77.15
$S—Me^2_i$	116.66	72.53	116.53	72.52	104.26	102.85

layer 2, confirming that layer 1 is more affected by the transition than layer 2. These environments are very similar to those reported for **2**, whatever the disordered cation and the temperature considered. This is also consistent with the stable physical behaviour of **2** upon cooling and tends to confirm that both phases are localised semiconductors at ambient pressure.

We may now return to the resistivity measurements under pressure carried out on phase **1** (see Fig. 5). Whereas the room temperature metal-like behaviour of **1** at ambient pressure had been convincingly associated with a 2D character of layer 2[11] it is likely that, under pressure, different metallic regimes could occur. The metal to insulator transition is indeed rather progressive and not reversible at ambient pressure, but it becomes more abrupt and reversible under pressure. In the low-temperature electronic structure of **1** (see Fig. 6b), one can notice the vicinity of the two partially filled bands to the Fermi level at point X. Even though a hydrostatic pressure is applied on the material, it is likely that its effect on both the intra- and the inter-chain interactions will not necessary be equivalent. Hence, two situations can arise, depending on whether the pressure enhances the one-dimensional inter-chain character of the anion layers (increasing mainly the ΓZ bandwidths) or lessens it (decreasing the bandwidths discrepancies between the ΓX and the ΓZ directions). In this latter case, a purely 2D metallic character could easily occur in the two layers of **1**, by contrast to what was observed at room temperature. Nevertheless, such a situation would suggest that the metal to insulator transition is associated with an electronic localisation at low temperatures, a fact that is not necessarily consistent with the more abrupt character of the transition when increasing the pressure. It seems thus more likely that a more pronounced one-dimensional character of the conductivity is provided by the pressure, together with a more rapid cation ordering. The metal to insulator transition could therefore be the result of a Peierls-like distortion, in agreement with a $q = 1/4a^* + 1/2c^*$ nesting vector. To confirm this hypothesis, it would be interesting to proceed with an X-ray diffraction study of **1** under pressure and check whether a metallic state is stabilised in **2** under pressure.

Concluding remarks

We have reported the synthesis, the room and low temperatures crystal structures, the resistivity measurements and the electronic band structures of two different $(SMeEt_2)[Pd(dmit)_2]_2$ phases. Although exhibiting identical stoichiometries, these two phases are structurally different and lead to different physical behaviours. The influence of the cationic disorder on the donor–acceptor electron transfers and therefore on the electrical properties of **1** and **2** provide new evidence of the key role of the counter-ions in the $M(dmit)_2$–based (M = Ni, Pd, Pt) molecular conductors.

Acknowledgements

T. T. thanks the Russian Foundation for Basic Research (RFBR) for supporting part of this work (grant 99-02-16119). Partial support from a CNRS-RAS PICS (N° 981) is gratefully acknowledged. D. Bérail, from Motorola, is acknowledged for supplying supports for conductivity measurements at ambient pressure.

References

1 P. Cassoux, L. Valade, H. Kobayashi, A. Kobayashi, R. A. Clark and A. E. Underhill, *Coord. Chem. Rev.*, 1991, **110**, 115.
2 P. Cassoux and L. Valade, in *Inorganic Materials*, 2nd Edition, ed. D. W. Bruce and D. O'Hare, Chichester, UK, 1996, p. 1.
3 E. Canadell, S. Ravy, J. P. Pouget and L. Brossard, *Solid State Commun.*, 1990, **75**, 633.
4 M. L. Doublet, E. Canadell, B. Garreau, J. P. Legros, L. Brossard, P. Cassoux and J. P. Pouget, *J. Phys.: Condens. Matter*, 1995, **7**, 4673.
5 A. Kobayashi, H. Kim, Y. Sasaki, K. Murata, R. Kato and H. Kobayashi, *J. Chem. Soc., Faraday Trans.*, 1990, **86**, 361.
6 C. Faulmann, J.-P. Legros, P. Cassoux, J. Cornelissen, L. Brossard, M. Inokuchi, H. Tajima and M. Tokumoto, *J. Chem. Soc., Dalton Trans.*, 1994, 249.
7 L. Brossard, H. Hurdequint, M. Ribault, L. Valade, J. P. Legros and P. Cassoux, *Synth. Met.*, 1988, **27**, B157.
8 L. Brossard, M. Ribault, L. Valade and P. Cassoux, *J. Phys.*, 1989, **50**, 1521.
9 M. Bousseau, L. Valade, J. P. Legros, P. Cassoux, M. Garbauskas and L. V. Interrante, *J. Am. Chem. Soc.*, 1986, **108**, 1908.
10 A. Kobayashi, A. Miyamoto, H. Kobayashi, A. Clark and A. E. Underhill, *J. Mater. Chem.*, 1991, **1**, 827.
11 C. Faulmann, A. Errami, B. Donnadieu, I. Malfant, J.-P. Legros, P. Cassoux, C. Rovira and E. Canadell, *Inorg. Chem.*, 1996, **35**, 3856.
12 G. Steimecke, H. J. Sieler, R. Kirmse and E. Hoyer, *Phosphorus, Sulfur Relat. Elem.*, 1979, **7**, 49.
13 Enraf-Nonius, *CAD4-Express Software*, Delft, The Netherlands, 1994.
14 Stoe and Cie, *IPDS Software, version 2.86*, Darmstadt, Germany, 1996.
15 L. J. Farrugia, *J. Appl. Crystallogr.*, 1999, **32**, 837.
16 A. Altomare, G. Cascarano, C. Giacovazzo and A. Guagliardi, *J. Appl. Cryst.*, 1993, **26**, 343.
17 G. M. Sheldrick, *SHELXL97- Programs for Crystal Structure Analysis (Release 97-2)*, Institüt für Anorganische Chemie der Universität, Tammanstrasse 4, D-3400 Göttingen, Germany, 1998.
18 D. M. Watkin, L. Pearce and C. K. Prout, *CAMERON - A Molecular Graphics Package*, Chemical Crystallography Laboratory, University of Oxford, 1993.
19 J. D. Thompson, *Rev.Sci.Instrum.*, 1984, **55**, 231.
20 R. J. Hoffman, *Chem. Phys.*, 1963, **39**, 1397.
21 J. H. Ammeter, H. B. Bürgi, J. Thibeault and R. J. Hoffman, *J. Am. Chem. Soc.*, 1978, **100**, 3688.
22 M. L. Doublet, E. Canadell, J. P. Pouget, E. B. Yagubskii, J. Ren and M. H. Whangbo, *Solid State Commun.*, 1993, **88**, 699.
23 As mentioned in the X-ray description of **1** at 160 K, the intramolecular distances reported for the two independent $Pd(dmit)_2$ units were shown to be rather different for the room-temperature crystal structure of **1**, in agreement with different fillings of their respective HOMO orbitals, and therefore with different fillings of the Y-HOMO-like bands of the two layers (see Table 2).